ASC Report No. 34/2013

Numerical simulation of the whispering gallery modes in prolate spheriods

P. Amodio, T. Levitina, G. Settani, E.B. Weinmüller

Institute for Analysis and Scientific Computing
Vienna University of Technology — TU Wien
www.asc.tuwien.ac.at ISBN 978-3-902627-05-6

Most recent ASC Reports

33/2013 *N. Zamponi and A. Jüngel*
Global existence analysis for degenerate energy-transport models for semiconductors

32/2013 *F. Achleitner, C.M. Cuesta, S. Hittmeir*
Travelling waves for a non-local Korteweg-de Vries-Burgers equation

31/2013 *T. Hohage, L. Nannen*
Convergence of infinite element methods for scalar waveguide problems

30/2013 *M. Feischl, T. Führer, M. Karkulik, J.M. Melenk, and D. Praetorius*
Quasi-optimal convergence rates for adaptive boundary element methods with data approximation,
Part II: Hyper-singular integral equation

29/2013 *W. Auzinger, A.S. Bagherzadeh, O. Koch*
Error estimation based on locally weighted defect for boundary value problems in second order ordinary differential equations

28/2013 *I.G. Graham, M. Löhndorf, J.M. Melenk, E.A. Spence*
When is the error in the h-BEM for solving the Helmholtz equation bounded independently of k ?

27/2013 *R. Hammer, W. Pötz, and A. Arnold*
Single-cone real-space finite difference scheme for the time-dependent Dirac equation

26/2013 *M. Aurada, M. Ebner, M. Feischl, S. Ferraz-Leite, T. Führer, P. Goldenits, M. Karkulik, M. Mayr, and D. Praetorius*
Hilbert (Release 3): A MATLAB implementation of adaptive BEM

25/2013 *M. Feischl, T. Führer, M. Karkulik, D. Praetorius, and E.P. Stephan*
Efficient additive Schwarz preconditioning
for hypersingular integral equations
on locally refined triangulations

24/2013 *M. Feischl, T. Führer, M. Karkulik, J.M. Melenk, and D. Praetorius*
Quasi-optimal convergence rates for adaptive boundary element methods with data approximation,
Part I: Weakly-singular integral equation

Institute for Analysis and Scientific Computing
Vienna University of Technology
Wiedner Hauptstraße 8–10
1040 Wien, Austria

E-Mail: admin@asc.tuwien.ac.at
WWW: http://www.asc.tuwien.ac.at
FAX: +43-1-58801-10196

ISBN 978-3-902627-05-6

Numerical simulation of the whispering gallery modes in prolate spheroids

P. Amodio[a], T. Levitina[b,*], G. Settanni[c], E. B. Weinmüller[d]

[a] *Dipartimento di Matematica, Università di Bari, Italy*
[b] *Institut Computational Mathematics, TU Braunschweig, Germany*
[c] *Dipartimento di Matematica e Fisica 'E. De Giorgi', Università del Salento, Italy*
[d] *Institute for Analysis and Scientific Computing, Vienna University of Technology, Austria*

Abstract

In this paper, we discuss the progress in the numerical simulation of the so-called 'whispering gallery' modes (WGMs) occurring inside a prolate spheroidal cavity. These modes are mainly concentrated in a narrow domain along the equatorial line of a spheroid and they are famous because of their extremely high quality factor. The scalar Helmholtz equation provides a sufficient accuracy for WGM simulation and (in a contrary to its vector version) is separable in spheroidal coordinates. However, the numerical simulation of 'whispering gallery' phenomena is not straightforward. The separation of variables yields two spheroidal wave ordinary differential equations (ODEs), first only depending on the angular, second on the radial coordinate. Though separated, these equations remain coupled through the separation constant and the eigenfrequency, so that together with the boundary conditions they form a singular self-adjoint two-parameter Sturm–Liouville problem.

We discuss an efficient and reliable technique for the numerical solution of this problem which enables calculation of highly localized WGMs inside a spheroid. The presented approach is also applicable to other separable geometries. We illustrate the performance of the method by means of numerical experiments.

*Corresponding author
Email addresses: pierluigi.amodio@uniba.it (P. Amodio), t.levitina@tu-braunschweig.de (T. Levitina), giuseppina.settanni@unisalento.it (G. Settanni), e.weinmueller@tuwien.ac.at (E. B. Weinmüller)

Keywords: Morphology dependent resonances, 'Whispering gallery' mode, Multiparameter spectral problems, Prüfer angle, High order finite difference schemes

1. Introduction and preliminaries

WGM resonators are of growing interest due to their exceptional properties, like an extremely high quality factor, or Q-factor, which indicates the rate of energy loss relative to the stored energy of the resonator. WGM resonators are encountered in numerous applications in science and industry, in such fields as optics and photonics [1].

An overview of the state of research on WGMs is provided in the recent publications [2, 3]. Although the theory of WGMs is well developed, the numerical simulation of these phenomena is not an easy task. The only exceptions are spherical and cylindrical resonators, for which precise calculations of eigenmodes, radiative losses, and field distributions are available [3, 4].

In the recent years, numerous attempts have been made to perform calculations of WGMs inside resonators of a non-spherical shape. In [5, 6] a direct finite-element simulation of WGMs inside ellipsoidal and toroidal resonators was presented. However, the limitations inherent in the finite-element approach do not allow to accurately calculate extremely highly localized oscillations.

If the shape of a resonator allows separation of variables in the modeling equation, this simplifies essentially both, the analytical and numerical analysis. Unfortunately, the above mentioned cases of a sphere and a cylinder expire the variety of separable geometries for the Helmholtz vector equation. However, WGMs inside spheroids may be still well modeled using the scalar Helmholtz equation [7], which is separable in spheroidal coordinates. A very detailed analysis of WGMs in spheroidal cavities given in [7] can be considered as a starting point of the present publication.

In the sequel, we report on a progress which we could achieve in the numerical simulation of WGMs occurring inside a prolate spheroid. Following the considerations in [7], the WGM phenomenon is simulated using the scalar Helmholtz equation. Either Dirichlet or Neumann boundary conditions are imposed on the boundary surface of the resonator and variables are separated in the prolate spheroidal coordinates. In the next section, we shall give an exact formulation of the problem arising thereby.

After the separation of variables, we obtain a system of ODEs (prolate spheroidal wave equations), depending on either angular or radial coordinate. These equations remain coupled via the separation constant and the eigenfrequency. Together with the boundary conditions they result in a singular self-adjoint two-parameter Sturm–Liouville problem.

The general theory of multi-parameter spectral problems is now well-developed [8, 9, 10]. Applied to the problem at hand, it guarantees the existence of a two-parameter eigenvalue and an associated two-component eigenfunction for any multi-index $(l,\, n)$, i.e. a pair of two non-negative integers l, n, indicating the number of oscillations of the eigenfunction components.

The multi-index $(l,\, n)$ and the azimuthal number m provide a very convenient opportunity to single out WGMs from the whole variety of oscillations inside a spheroid. WGMs are modes corresponding to small indices l and n $(l, k \sim 0 - 3)$ and extra large azimuthal numbers $m \sim 1000 - 10000$.

Even in the simplest cases numerical solution of a singular two-parameter Sturm–Liouville problem requires special care. First we transfer those boundary conditions which are necessary and sufficient for the solution to stay bounded, from the singular points to the close regular points, see [11, 12]. In the second step, we apply to such a 'regularized problem' a properly modified algorithm developed in [13] for the evaluation of the angular ellipsoidal (Lamé) wave functions. This algorithm is based on the WKB asymptotics[1] of the bounded solutions of the prolate spheroidal wave equations, i.e. on the related Prüfer angles, and it allows calculation of even extremely rapidly oscillating solutions. Yet, in the WGMs case, the rapidly oscillating angular azimuthal component is known *a priori*, while the evaluated components practically do not oscillate: they vanish on a large part of their domain and change sharply only in a very narrow subinterval. This restricts the computational accuracy of the Prüfer angles in case of the low-oscillatory components, and the calculations may become unstable. In spite of that, the Prüfer angle can be used to localize the desired eigenvalue and to provide a very accurate initial guess for a subsequent calculation of the desired WGMs using the Newton's iteration. The latter is carried out after the discretzation of the spheroidal wave equations based on the high-order difference schemes

[1] An asymptotic method introduced by G. Wentzel, H. Kramers, L. Brillouin, and H. Jeffreys to obtain approximate solutions of Schrödinger equation. For a detailed historical account and literature see e.g. [14].

and provide very accurate approximation for both, the WGM eigenfrequency and the associated solution of the scalar Helmholtz equation.

2. Prolate spheroidal coordinates and prolate spheroidal wave functions

In this section we collect the most important facts concerning the problem setting. For more details see [7, 15] and the literature therein.

Prolate spheroidal coordinates are introduced via their relations to the conventional Cartesian coordinates,

$$x = \frac{d}{2}\sqrt{(\xi^2-1)(1-\eta^2)}\cos\varphi, \quad y = \frac{d}{2}\sqrt{(\xi^2-1)(1-\eta^2)}\sin\varphi, \quad z = \frac{d}{2}\xi\eta,$$

where $\varphi \in [0,\ 2\pi)$ is the azimuthal angle, while $\eta \in (-1, 1)$ and $\xi \in (1, \infty)$ play the roles of inclination and radius, respectively. The corresponding coordinate surfaces are confocal two-sheeted hyperboloids of revolution and prolate spheroids, with d being the distance between the foci.

The eigenvalue problem for the Laplace operator defined on the domain bounded by a spheroid $\xi = \xi_s$,

$$-\Delta\, W(\mathbf{r}) = k^2\, W(\mathbf{r}), \quad \mathbf{r} = (\varphi, \eta, \xi), \quad \xi < \xi_s,$$

is separable in spheroidal coordinates, provided that either Dirichlet or Neumann boundary conditions are imposed. Any particular solution of the problem is represented as a product of its angular, radial and azimuthal part,

$$W(\mathbf{r}) = S(\eta)R(\xi)\exp(\pm i\, m\, \varphi), \quad m = 0, 1, \ldots.$$

Here $S(\eta)$ and $R(\xi)$ are bounded solutions of the angular and radial prolate spheroidal wave equations, respectively,

$$\frac{d}{d\eta}(1-\eta^2)\frac{d}{d\eta}S \ + \ \left[\lambda + c^2(1-\eta^2) - \frac{m^2}{1-\eta^2}\right] S = 0, \quad -1 < \eta < 1, \quad (1)$$

$$\frac{d}{d\xi}(\xi^2-1)\frac{d}{d\xi}R \ + \ \left[c^2(\xi^2-1) - \lambda - \frac{m^2}{\xi^2-1}\right] R = 0, \quad 1 < \xi < \xi_s. \quad (2)$$

Note that the differential operator in (1) exhibits two singular points at $\eta = \pm 1$, while equation (2) has a singular point $\xi = 1$.

Due to the symmetry of the problem, one can consider (1) on the half-interval $[0, 1)$, requiring the angular function $S(\eta)$ to be either odd or even, and satisfying respectively, the following initial condition:

$$S(0) = 0, \quad S'(0) = 0. \tag{3}$$

The boundary condition on the surface of the spheroid implies for the radial function $R(\xi)$ that either one of the following terminal conditions holds:

$$R(\xi_s) = 0, \quad R'(\xi_s) = 0. \tag{4}$$

Solutions of the system (1), (2) bounded at singular points $\eta = 1$ and $\xi = 1$ satisfy the boundary conditions (3), (4) not for all λ and c^2. If for a pair (λ, c^2) there exists a bounded non-trivial solution to each of the problems (1), (3) and (2), (4), such a pair is called a two-parameter eigenvalue of the system. Hereafter, we specify eigenvalues (λ, c^2) with a multi-index (l, k), in which the integers l and k count the numbers of internal zeros of the associated angular and radial functions, $S_{lk}(\eta)$ and $R_{lk}(\xi)$, inside the intervals $(-1, 1)$ and $(1, \xi_s)$. Note that the parity of the index l defines the parity of the angular function S_{lk}.

In addition, functions $S_{lk}(\eta)$ and $R_{lk}(\xi)$ are normalized by

$$\int_{-1}^{1} S_{lk}^2(\eta)\, d\eta \;=\; 1, \quad \int_{1}^{\xi_s} R_{lk}^2(\xi)\, d\xi \;=\; 1. \tag{5}$$

In the sequel, the multi-index $(l,\, k)$ as well as the azimuthal number m are fixed, and $m > 0$. Although the case $m = 0$ does not cause any additional difficulty, it should be considered separately. Here, we omit this case, since it plays no role in the simulation of the 'whispering gallery' phenomenon.

3. Boundary conditions transferred to a regular point

The numerical technique presented below is not applicable to singular boundary value problems, therefore we shall formulate an equivalent regular boundary value problem on the domain $(0,\ 1-\delta_\eta) \times (1+\delta_\xi,\ \xi_s)$ with $\delta_\eta > 0$ and $\delta_\xi > 0$ chosen to exclude singular points from the integration interval.

Let us first consider equation (1). Here, the singularity at the point $\eta = 1$ is indeed regular [16]. Unless $m = 0$, any bounded solution of (1) behaves as [15],

$$S(\eta) \sim (1 - \eta^2)^{m/2}, \quad \eta \to 1- \ .$$

For (2), the singularity at the point $\xi = 1$ is again regular; for a solution bounded at $\xi = 1$ the following asymptotic holds:

$$R(\xi) \sim (\xi^2 - 1)^{m/2}, \quad \xi \to 1+ \ .$$

All solutions of (1) bounded at $\eta = 1$ possess the same (modified) logarithmic derivative $\beta_a(\eta)$ defined by

$$(1 - \eta^2)\frac{d}{d\eta}S(\eta) = \beta_a(\eta)\, S(\eta). \tag{6}$$

One can prove that $\beta_a(\eta)$ is a holomorphic solution of the Riccati equation,

$$\beta_a' + \frac{\beta_a^2}{1 - \eta^2} + Q_a(\eta) = 0, \quad Q_a(\eta) := \lambda + c^2(1 - \eta^2) - \frac{m^2}{1 - \eta^2},$$

such that $\lim_{\eta \to 1-0} \beta_a(\eta) = -m$. In the vicinity of $\eta = 1$, it can be represented in form of an absolutely and uniformly convergent series,

$$\beta_a(\eta) = \sum_{k=0}^{\infty} \beta_k (1 - \eta)^k, \tag{7}$$

with known coefficients; see [11, 12] for details. Thus (6) transfers the condition necessary for the solution to stay bounded from the singular point $\eta = 1$ to a closely located regular one, $\eta = 1 - \delta_\eta$.

The holomorphic solution

$$\beta_r(\xi) = \sum_{k=0}^{\infty} \tilde{\beta}_k (\xi - 1)^k \tag{8}$$

of the equation

$$\beta_r' + \frac{\beta_r^2}{1 - \xi^2} + Q_r(\xi) = 0, \quad Q_r(\xi) := c^2(1 - \xi^2) - \lambda - \frac{m^2}{1 - \xi^2},$$

serves to transfer the analogous condition for the radial function to a close regular point $\xi = 1 + \delta_\xi$,

$$(\xi^2 - 1)\frac{d}{d\xi}R(\xi) = \beta_r(\xi)\, R(\xi). \tag{9}$$

In [11, 12] the convergence radii σ_η and σ_ξ are specified, as well as the upper bound for the truncations errors in the series (7) and (8).

Let us recapitulate: We substitute the original boundedness conditions at the singular points of equations (1) and (2) by the following boundary conditions posed at regular points, $\eta = 1 - \delta_\eta$ and $\xi = 1 + \delta_\xi$, with $\delta_\eta < \sigma_\eta$ and $\delta_\xi < \sigma_\xi$:

$$\delta_\eta(2 - \delta_\eta)S'(1 - \delta_\eta) = \hat{\beta}_a(1 - \delta_\eta)\, S(1 - \delta_\eta), \tag{10}$$

$$\delta_\xi(2 + \delta_\xi)R'(1 + \delta_\xi) = \hat{\beta}_r(1 + \delta_\xi)\, R(1 + \delta_\xi). \tag{11}$$

Here, $\hat{\beta}_a$ and $\hat{\beta}_r$ are the appropriately truncated expansions (7) and (8), respectively.

4. Numerical search technique for two-parameter spectral problems

In [13] a method for evaluating the ellipsoidal angular (Lamé) wave functions was proposed. These functions are eigenfunctions of a two-parameter singular self-adjoint Sturm–Liouville problem, which arises when in the Helmholtz equation variables are separated in ellipsoidal coordinates. The search for a two-parameter eigenvalue was implemented by means of a globally converging procedure. The condition for the applicability of this procedure is the monotone dependence of the equation coefficients on the spectral parameters. The coefficients in equations (1) and (2) show the required monotonicity and the numerical approach discussed in [13] can be applied to compute the eigenvalue $(\lambda, c^2)_{lk}$.

Let us now sketch the main idea of the eigenvalue search.

Consider (1) on the half-interval $(0, 1 - \delta_\eta)$ together with the boundary conditions (3) and (10). For any given value of c^2, the general theory guarantees the existence of the value $\lambda = \lambda_l^a(c^2)$, such that a non-trivial solution of the problem (1), (3), (10) exists, which oscillates l times inside $(-1 + \delta_\eta, 1 - \delta_\eta)$. Since $Q_a(\eta)$ monotonically increases with both λ and c^2, the dependence $\lambda = \lambda_l^a(c^2)$ is monotonically decreasing.

Moreover, let the value $\lambda = \lambda_k^r(c^2)$ be such that a non-trivial solution of the problem (2), (4), (11) exists, which oscillates n-times on $(1 + \delta_\xi, \xi_s)$. Then $\lambda = \lambda_k^r(c^2)$ increases monotonically with growing c^2. Obviously, the intersection point of the spectral curves $\lambda = \lambda_l^a(c^2)$ and $\lambda = \lambda_k^r(c^2)$ is the desired eigenvalue $(\lambda, c^2)_{lk}$. The spectral curves subdivide the plane λ, c^2

into four sub-domains, in which the points (λ, c^2) are either above/below the eigenvalue $(\lambda, c^2)_{lk}$, or left/right of it.

The key role in the related calculations is played by the Prüfer angle – an auxiliary function introduced to single out solutions of (1) and (2) bounded at singular points. The Prüfer angles $\theta_a(\eta)$ and $\theta_r(\xi)$ relate in a simple way to the logarithmic derivatives $\beta_a(\eta)$ and $\beta_r(\xi)$: $\tan\theta_i(\cdot) = -\beta_i(\cdot)$, $i = a, r$. At any point of the spectral plane (λ, c^2) one can compute these functions integrating the equations

$$\theta_a{}' = \frac{\sin^2(\theta_a)}{(1-\eta^2)} + \mathrm{Q_a}(\eta)\cos^2(\theta_a) \quad \eta \in (0, 1-\delta_\eta), \tag{12}$$

$$\theta_r{}' = \frac{\sin^2(\theta_r)}{(\xi^2-1)} + \mathrm{Q}_r(\eta)\cos^2(\theta_r), \quad \xi \in (1+\delta_\xi, \xi_s), \tag{13}$$

with the initial conditions

$$\theta_a(1-\delta_\eta) = \arctan\left(\beta_a(1-\delta_\eta)\right), \quad \theta_r(1+\delta_\xi) = \arctan\left(\beta_r(1+\delta_\xi)\right). \tag{14}$$

Then for the bounded solutions of equations (1) and (2) the following equalities hold:

$$\begin{aligned} S(\eta)\ \sin\left(\theta_a(\eta)\right) &+ (1-\eta^2)\ S'(\eta)\ \cos\left(\theta_a(\eta)\right) = 0, \quad \eta \in (0, 1-\delta_\eta), \\ R(\xi)\ \sin\left(\theta_r(\xi)\right) &+ (\xi^2-1)\ R'(\xi)\ \cos\left(\theta_r(\xi)\right) = 0, \quad \xi \in (1+\delta_\xi, \xi_s). \end{aligned}$$

Each time when either $S(\eta)$ or $R(\xi)$ vanishes, the Prüfer angle $\theta_a(\eta)$ or $\theta_r(\xi)$ crosses a line $\theta = n\pi + \dfrac{\pi}{2}$, thereby increasing in agreement with (12). Therefore θ_a and θ_r count the numbers of zeros that the related solutions have between the interval endpoint and the current argument value.

Denote

$$\Delta_a(\lambda, c^2, l) = \theta_a(0) - \frac{l\pi}{2},$$

$$\Delta_r(\lambda, c^2, k) = \theta_r(\xi - s) - \begin{cases} k\pi, & \text{for the Dirichlet condition (4)}, \\ \left(k + \dfrac{1}{2}\right)\pi, & \text{for the Neumann condition (4)}. \end{cases}$$

The point (λ, c^2) is the desired eigenvalue of the multi-index (l, k) iff

$$\Delta_a(\lambda, c^2, l) = \Delta_r(\lambda, c^2, k) = 0.$$

Moreover, for an arbitrary point (λ, c^2) one can prove that

$$\begin{aligned} \operatorname{sign}\left(\lambda - \lambda_l^a(c^2)\right) &= \operatorname{sign}\left(\Delta_a(\lambda, c^2, l)\right), \\ \operatorname{sign}\left(\lambda - \lambda_k^r(c^2)\right) &= \operatorname{sign}\left(\Delta_r(\lambda, c^2, k)\right). \end{aligned} \tag{15}$$

This means that the signs of $\Delta_a(\lambda, c^2, l)$, $\Delta_r(\lambda, c^2, k)$ indicate to which of the above sub-domains the point (λ, c^2) belongs. Varying properly values of λ and c^2, one finds a point in each of the sub-domains: $(\lambda, c^2)^{(++)}$, $(\lambda, c^2)^{(-+)}$, $(\lambda, c^2)^{(--)}$, and $(\lambda, c^2)^{(+-)}$, where the signs in the upper index are the same as of $\Delta_a(\lambda, c^2, l)$, $\Delta_r(\lambda, c^2, k)$. The rectangle formed by the lines $\lambda = \lambda^{(++)}$, $c^2 = c^{2(-+)}$, $\lambda = \lambda^{(--)}$, $c^2 = c^{2(+-)}$, contains the eigenvalue $(\lambda, c^2)_{lk}$.

After the eigenvalue is captured in a rectangle, it can be accurately computed by a bisection method: depending on the domain, in which the center of a capturing rectangle is located (i.e. above-below or to the left-right of the eigenvalue), the empty half of a rectangle is neglected. We repeat calculations until the accuracy becomes satisfactory.

We emphasize that the eigenvalue is computed for an *a priory* chosen multi-index. The procedure converges globally, regardless of the initial guess (λ, c^2). The spectral curves, $\lambda = \lambda_l^a(c^2)$ and $\lambda = \lambda_k^r(c^2)$, though involved in the calculations, are not computed.

In the practical calculations we use a modification of the conventional Prüfer angle, which is free from the well-known drawback – the stepwise behavior – yet keeping on the possibility to count the number of zeros. For more details we refer to [12].

When separating the variables, the coefficients of the decomposed equations may not satisfy the monotonicity requirement. Still, under certain conditions [8] the above procedure can be applied after an appropriate change of the spectral parameters [17]. The presented approach was generalized to three-parameter problems in [18].

5. Finite difference schemes for the hyper-spheroidal function

The Prüfer angle technique is based on the WKB [19] asymptotics that mimic an oscillating solution of a second order ODE. The higher the number of oscillations is, the larger the benefit of the method.

However, in the present work we are interested in the modes adjacent to the surface of the spheroid in the equatorial plane. In terms of the separated equations, this means that the turning points η_T and ξ_T of (1), (2), i.e. the

points in which the potentials $Q_a(\eta)$ and $Q_r(\xi)$ change their signs, are very close to 0 and ξ_s, respectively. If this is the case, the eigenfunctions $S_{lk}(\eta)$ and $R_{lk}(\xi)$ do not oscillate on most of their definition intervals, namely on $(\eta_T, 1)$ and on $(1, \xi_T)$. Instead, they decay there exponentially fast. The oscillations are then concentrated inside the very narrow intervals $(0, \eta_T)$ and (ξ_T, ξ_s). Even for small indexes l, k the functions $S_{lk}(\eta)$ and $R_{lk}(\xi)$ change in an extremely sharp way (see Figure 1(a)). As a result, the accuracy of the Prüfer angle calculations deteriorates with growing m and small l, k. Fortunately, in spite of the unstable behavior, the above approach still allows to localize the eigenvalues and provide a very accurate initial guess for the Newton iteration applied to the nonlinear discrete problem arising after discretization of the ODE system [20].

We discretize the BVP (1), (2), (10), (11) using high order finite differences (see [21, 22]). To explain the procedure, let us, for simplicity, consider a system of second order ODEs,

$$f(x, y, y', y'') = 0, \quad x \in [a, b], \tag{16}$$

subject to two boundary conditions defined in $x = a$ and $x = b$. First, the interval $[a, b]$ is subdivided uniformly in $n - 1$ subintervals, where the grid points are $x_i = a+(i-1)h$, $i = 1, \ldots, n$, with the stepsize $h = (b-a)/(n-1)$. The derivatives are approximated in x_i utilizing the formulae

$$y^{(\nu)}(x_i) \approx y_i^{(\nu)} = \frac{1}{h^\nu} \sum_{j=-s}^{r} \alpha_{j+s}^{(\nu)} y_{i+j}, \quad \nu = 1, 2, \tag{17}$$

where the coefficients $\alpha_{j+s}^{(\nu)}$ of the method are computed to guarantee the highest possible order of consistency.

Now, we have to solve a closed system with n equations for n unknowns y_i, $i = 1, \ldots, n$. For a general BVP we arrive at a nonlinear algebraic system of equations,

$$F(x_i, y_i, y_i', y_i'') = 0, \quad i = 2, \ldots, n-1, \tag{18}$$

subject to boundary conditions. If $r = s$, formulae (17) are of order $p = 2r$ (otherwise, the order is $p = r + s - \nu + 1$) and have good stability properties. Therefore, we choose p even and approximate $y_i^{(\nu)}$ by $s = r = p/2$ when $i \geq p/2$ and $i \leq n - p/2$. In the initial points, $i < p/2$, we choose $s = i$ and $r = p - s + \nu - 1$, since left of x_i there are not $p/2$ values available. Analogously, for $i > n - p/2$, we choose $r = n - i$ and $s = p - r + \nu - 1$.

Hence, in a block form each derivative is approximated by $Y^{(\nu)} = A_\nu Y$, where A_ν is a banded matrix [23].

For regular second order BVPs for ODEs with appropriately smooth solution, the global error order of the above finite difference scheme coincides with the order of consistency [21].

To numerically simulate the two-parameter Sturm-Liouville problem (1), (2), (10), (11), whose solution satisfies (5), we use n_1 and n_2 equidistant points on two integration intervals $[0,\ 1-\delta_\eta]$ and $[1+\delta_\xi, \xi_s]$, respectively. Hence, the resulting nonlinear system consists of $n_1 + n_2 + 2$ equations for the following unknowns: $S(\eta_i)$, for $i = 1, \ldots, n_1$, $R(\xi_i)$, for $i = 1, \ldots, n_2$, and the eigenvalues λ and c^2. Let S and R consist of the discrete values for $S(\eta_i)$ and $R(\xi_i)$, then the discrete problem can be written as

$$\begin{aligned}
&((I - D_\eta^2)A_1 - 2D_\eta A_2 + \lambda I + c^2(I - D_\eta^2) - m^2(I - D_\eta^2)^{-1})S = 0,\\
&((D_\xi^2 - I)A_1 + 2D_\xi A_2 + c^2(D_\xi^2 - I) - \lambda I - m^2(D_\xi^2 - I)^{-1})R = 0,\\
&h_1 S^T D_1 S = 0, \quad h_2 R^T D_2 R = 0.
\end{aligned} \tag{19}$$

Here, the diagonal matrices D_x include the values x_i for $x = \eta, \xi$, D_1 and D_2 are the diagonal matrices resulting from the quadrature formulae approximating the normalization conditions (5). In the matrices A_1 and A_2 the coefficients of the method are stored and h_i, $i = 1, 2$, are the stepsizes.

To solve system (19), we proceed as follows. First of all we compute an initial approximation of λ and c^2 using the Prüfer angle technique and substitute these values into (19). Then system (19) is decoupled into two subsystems,

$$((I - D_\eta^2)A_1 - 2D_\eta A_2 + \lambda I + c^2(I - D_\eta^2) - m^2(I - D_\eta^2)^{-1})S = 0, \tag{20}$$

$$h_1 S^T D_1 S = 0, \tag{21}$$

and

$$((D_\xi^2 - I)A_1 + 2D_\xi A_2 + c^2(D_\xi^2 - I) - \lambda I - m^2(D_\xi^2 - I)^{-1})R = 0, \tag{22}$$

$$h_2 R^T D_2 R = 0, \tag{23}$$

with $n_1 + 1$ and $n_2 + 1$ equations, respectively. Note that linear systems (20) and (22) are singular and therefore, there exist infinitely many solutions

S and R. To overcome this difficulty, we utilize the knowledge about the analytical solution of (1) and (2) which allows us to localize a non-zero component in S and R. We set these components to 1 and compute the other components uniquely from (20) and (22). Now, (21) and (23) are used to normalize S and R. At this stage, preliminary approximations for λ, c^2, S and R are available. In the final phase, we apply the Newton method to the whole system (19) in order to improve the preliminary solution. The tolerance for the Newton iteration was set to 10^{-11} and achieved within 10 iteration steps.

6. Numerical experiments

In the numerical solution of (1), (2), (5), (10), (11), we focus our attention on the case of large azimuthal number m and small numbers of oscillations l and k. Since, the accuracy of the Prüfer angle calculations is not satisfactory in this case, we have developed a MATLAB code based on the finite difference schemes introduced in the previous section. The code utilizes schemes of order 4, 6 and 8. Since the exact solution is not available, we use the approximations obtained with the method of order 8 and $n_1 = n_2 = 16000$ as reference solutions $(\tilde{\lambda}, \tilde{c}^2)$ for the eigenvalues and $(\tilde{S}(\eta), \tilde{R}(\xi))$ for the eigenfunctions.

We are interested to observe the performance of our code, especially its accuracy. Starting with $n_1 = n_2 = 250$ equidistant grid points and doubling their number step by step, we estimate the relative errors in the eigenvalues from the following formulae:

$$Err_\lambda = \left| \frac{\lambda - \tilde{\lambda}}{\tilde{\lambda}} \right|, \quad Err_{c^2} = \frac{|c^2 - \tilde{c}^2|}{\tilde{c}^2}.$$

For the eigenfunctions, to avoid division by zero, we measure the relative errors via the following expressions:

$$Err_S = \max_\eta \frac{|S(\eta) - \tilde{S}(\eta)|}{1 + |\tilde{S}(\eta)|}, \quad Err_R = \max_\xi \frac{|R(\xi) - \tilde{R}(\xi)|}{1 + |\tilde{R}(\xi)|},$$

where the maximum is taken over the grid points.

The numerical results shown in Figures 1 to 4 are for schemes of order 6, $l = 2$, $n = 0$ and for the following values of m and ξ_s:

1. $m = 500$, $\xi_s = 1.1$.
2. $m = 1000$, $\xi_s = 1.1$.
3. $m = 2000$, $\xi_s = 1.1$.
4. $m = 2000$, $\xi_s = 1.5$.

Figure 1 also includes the eigenfunctions S and R and a 3D plot of the solution. Note, that in Figure 1(a), the scaling is such that the vicinity of the interval ends is 'zoomed in'. In fact the functions S and R are very much steeper at the left and right boundary, respectively, than it appears at the first glance. The plots associated with the other cases exhibit similar behaviour. Comparing problems with the same number of oscillations in S and R, we observe that larger values of m require smaller stepsizes for the same accuracy. This is not surprising, because for large values of m, the contribution to the singular terms in $Q_a(\eta)$ and $Q_r(\xi)$ becomes correspondingly large. In all cases we are able to provide solutions whose error is smaller than 10^{-12}.

As a further test, Figure 5 shows the relative errors of the eigenvalue λ calculated for $l = 2$, $n = 0$, $m = 500$, $\xi_s = 1.1$, using schemes of order 4, 6 and 8. The experimentally computed order is in a good agreement with the theoretical one, until the round-off error level is reached. Similar behaviour has been observed for c^2.

In Tables 1 and 2, we display the first 9 (exact) digits of the eigenvalues computed for large m and small ξ_s, l and k, for both, Dirichlet and Neumann boundary conditions. The approximations obtained via the Prüfer angle provide values with 6 accurate digits. These reference solutions are listed for possible further comparisons.

Conclusions

We discussed 'internal boundary value problems' in context of scalar Helmholtz equation describing free oscillation inside a resonator cavity. For prolate spheroids, the Helmholtz equation can be rewritten as a two-parameter self-adjoint Sturm–Liouville problem. We developed an efficient and reliable numerical technique for simulating and investigating oscillations inside prolate spheroids. In particular, we were able to calculate highly localized 'whispering gallery modes'. The proposed technique provides accurate results for a wide range of input parameters and its advantage is, that the calculations are performed for an eigenfrequency of a desired multi-index.

This approach is applicable for any other separable geometry.

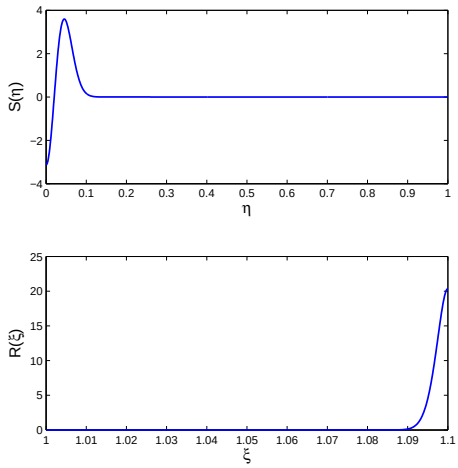

(a) *Eigenfunctions*

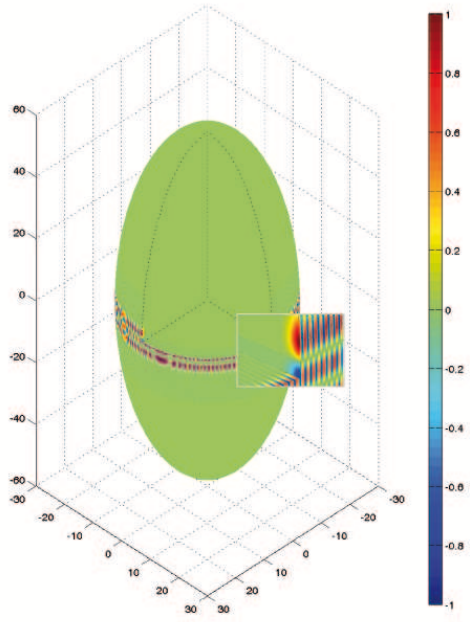

(b) *3D solution*

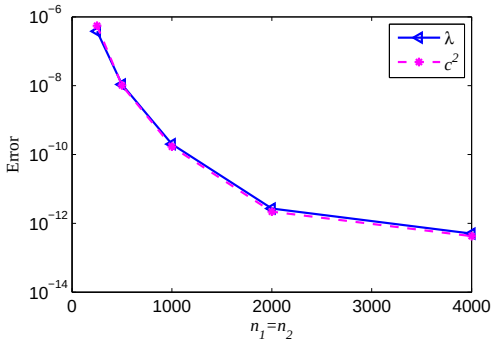

(c) *Errors of the eigenvalues,* Err_λ *and* Err_{c^2}

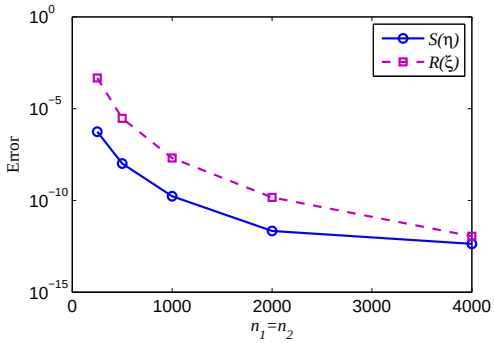

(d) *Errors of the eigenfunctions,* Err_S *and* Err_R

Figure 1: Whispering gallery mode: $m = 500$, $l = 2$, $n = 0$, $\xi_s = 1.1$, $S'(0) = 0$, $R'(\xi_0) = 0$, $\tilde{\lambda} = -9.70206330e + 05$, $\tilde{c}^2 = 1.22627934e + 06$.

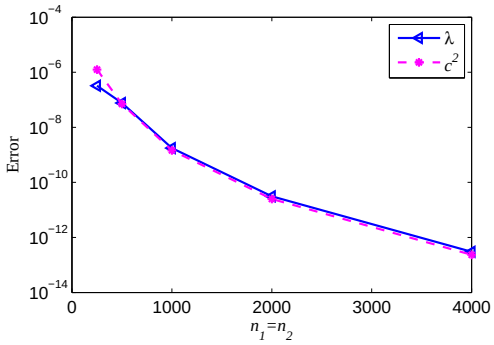

(a) *Errors of the eigenvalues,* Err_λ *and* Err_{c^2}

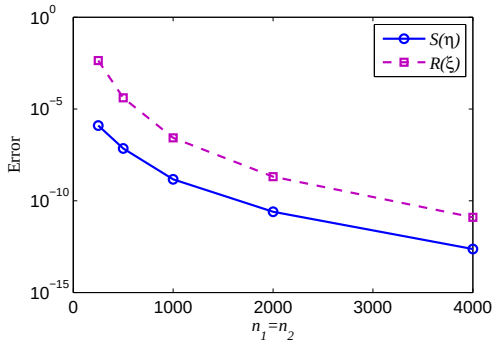

(b) *Errors of the eigenfunctions,* Err_S *and* Err_R

Figure 2: Whispering gallery mode: $m = 1000$, $l = 2$, $n = 0$, $\xi_s = 1.1$, $S'(0) = 0$, $R'(\xi_0) = 0$, $\tilde{\lambda} = -3.83716546e + 06$, $\tilde{c}^2 = 4.84925600e + 06$.

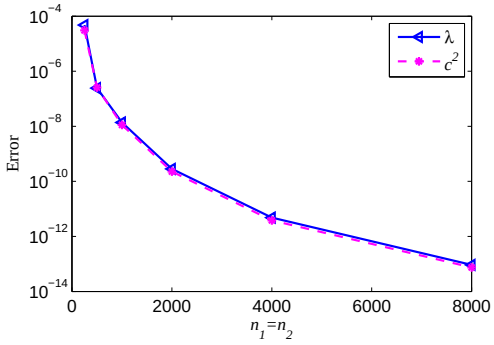

(a) *Errors of the eigenvalues,* Err_λ *and* Err_{c^2}

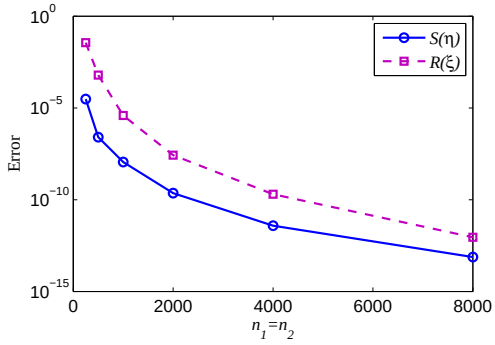

(b) *Errors of the eigenfunctions,* Err_S *and* Err_R

Figure 3: Whispering gallery mode: $m = 2000$, $l = 2$, $n = 0$, $\xi_s = 1.1$, $S'(0) = 0$, $R'(\xi_0) = 0$, $\tilde{\lambda} = -1.52380361e + 07$, $\tilde{c}^2 = 1.92621494e + 07$.

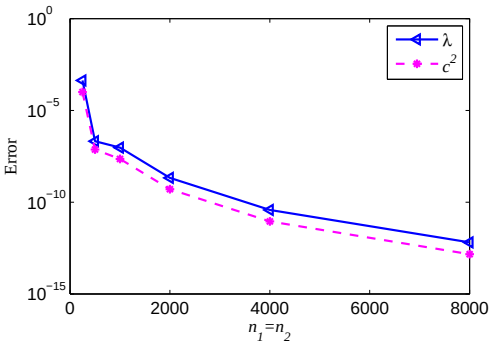

(a) *Errors of the eigenvalues,* Err_λ *and* Err_{c^2}

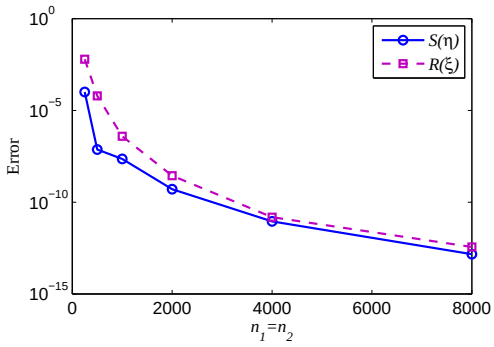

(b) *Errors of the eigenfunctions,* Err_S *and* Err_R

Figure 4: Whispering gallery mode: $m = 2000$, $l = 2$, $n = 0$, $\xi_s = 1.5$, $S'(0) = 0$, $R'(\xi_0) = 0$, $\tilde{\lambda} = 7.74792856e + 05$, $\tilde{c}^2 = 3.23866116e + 06$.

m	ξ_s	l	n	$\tilde{\lambda}$	$\tilde{c^2}$
1000	1.01	0	0	-5.06252341e+07	5.16324882e+07
1000	1.1	0	0	-3.94087190e+06	4.94330917e+06
1000	1.1	0	1	-4.07862082e+06	5.08108618e+06
1000	1.1	0	2	-4.19366290e+06	5.19615148e+06
1000	1.1	1	0	-3.94004236e+06	4.94735740e+06
1000	1.1	1	1	-4.07779423e+06	5.08519355e+06
1000	1.1	2	0	-3.93921234e+06	4.95140798e+06
2000	1.1	0	1	-1.58382777e+07	1.98431600e+07
2000	1.1	0	2	-1.61217871e+07	2.01266984e+07
2000	1.1	1	0	-1.54946648e+07	1.95092096e+07
2000	1.1	1	1	-1.58366199e+07	1.98512701e+07
2000	1.1	2	0	-1.54930027e+07	1.95172479e+07

Table 1: Numerical results for Dirichlet boundary conditions

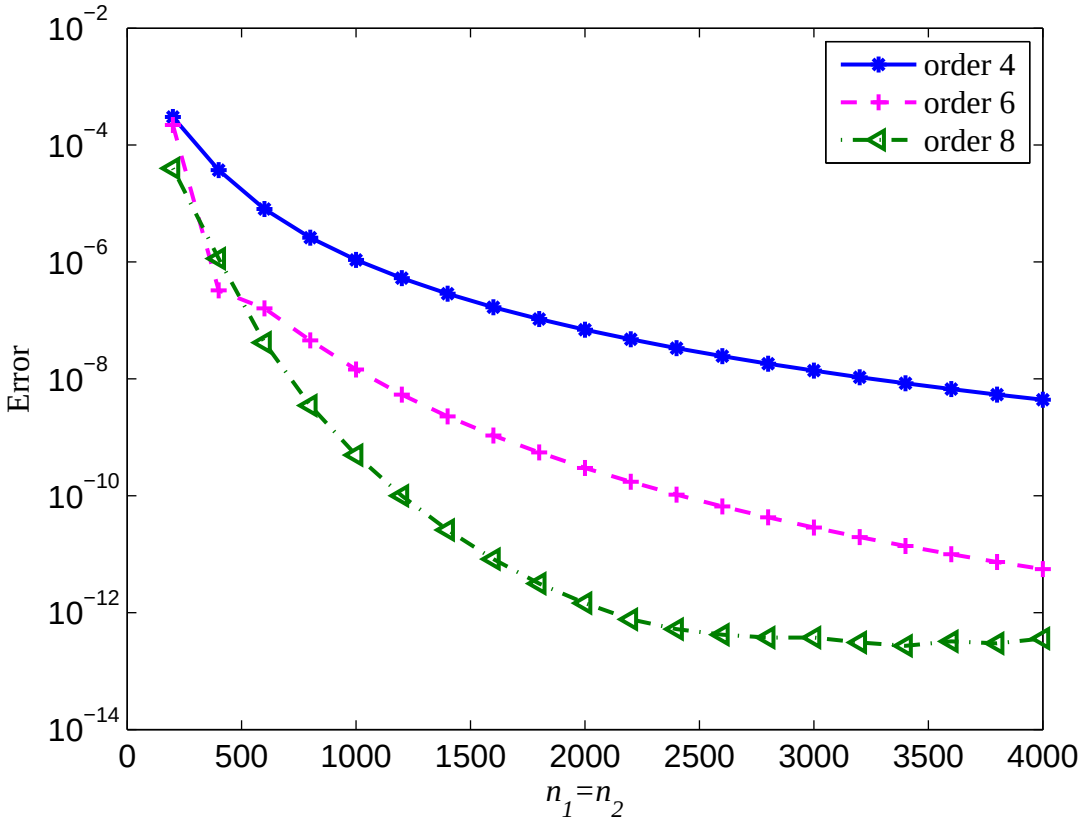

Figure 5: Relative errors for the eigenvalue λ, $m = 500$, $l = 2$, $n = 0$, $\xi_s = 1.1$, $S'(0) = 0$, $R'(\xi_0) = 0$

m	ξ_s	l	n	$\tilde{\lambda}$	$\tilde{c^2}$
1000	1.01	0	0	-4.95596121e+07	5.05667923e+07
1000	1.1	0	0	-3.83882970e+06	4.84124594e+06
1000	1.1	0	1	-4.01208260e+06	5.01453443e+06
1000	1.1	0	2	-4.13711981e+06	5.13959701e+06
1000	1.1	1	0	-3.83799783e+06	4.84524980e+06
1000	1.1	1	1	-4.01125461e+06	5.01861334e+06
2000	1.1	0	0	-1.52413658e+07	1.92461866e+07
2000	1.1	0	1	-1.56734959e+07	1.96783613e+07
2000	1.1	0	2	-1.59827081e+07	1.99876052e+07
2000	1.1	1	0	-1.52397012e+07	1.92541669e+07
2000	1.1	1	1	-1.56718363e+07	1.96864358e+07

Table 2: Numerical results for Neumann boundary conditions

Acknowledgements

The authors gratefully acknowledge the warm hospitality of Vienna University of Technology.

References

[1] V.S. Ilchenko and A.B. Matsko, Optical resonators with whispering gallery nodes — Part II: Applications, *IEEE J. Sel. Topics Quantum Electron.* **12** (2006), 15–32.

[2] A.B. Matsko and V.S. Ilchenko, Optical resonators with whispering gallery nodes — Part I: basics, *IEEE J. Sel. Topics Quantum Electron.* **12** (2006), 3–14.

[3] A.B. Matsko, A.A. Savchenkov, D. Strekalov, V.S. Ilchenko, and L. Maleki, Review of Applications of Whispering-Gallery Mode Resonators in Photonics and Nonlinear Optics, *IPN PR – Nasa* **42-162** (2005), 1–51.

[4] M.L. Gorodetsky and V.S. Ilchenko, High-Q optical whisperinggallery microresonators: Precession approach for spherical mode analysis and emission patterns with prism couplers, *Opt. Comm.* **113** (1994), 133–143.

[5] A. Aiello and M. Ornigotti, Theory of Anisotropic Whispering Gallery Resonators, arxiv:1107.2044

[6] M. Oxborrow, Traceable 2-D finite-element simulation of the whispering-gallery modes of axisymmetric electromagnetic resonators, *IEEE Trans. Microw. Theory Tech.* **55** (2007), 1209–1218.

[7] M.L. Gorodetsky and A.E. Fomin, Geometrical Theory of Whispering-Gallery Modes, *IEEE J. Sel. Top. Quantum Electron.* **12** (2006), 33–39.

[8] B.D. Sleeman, Multiparameter Spectral Theory in Hilbert Space, (Research Notes in Mathematics vol 22), London: Pitman, 1978.

[9] B.D. Sleeman, Multiparameter spectral theory and separation of variables, *J.* Phys. A: Mathematical Theory **41** (2008), 1–20.

[10] H. Volkmer, Multiparameter Eigenvalue Problems and Expansion Theorems, *Lecture Notes in Mathematics* **1356**, Springer-Verlag, Berlin, New York, 1988.

[11] A.A. Abramov, A.L. Dyshko, and N.B. Konyukhova, Computation of Prolate Spheroidal Functions by Solving the Corresponding Differential Equations, *U.S.S.R. Comput. Math. Math. Phys.* (1984) **24**, 1–11.

[12] T.V. Levitina and E.J. Brändas, Computational techniques for Prolate Spheroidal Wave Functions in Signal Processing, *J. Comp. Meth. Sci. & Engrg.* **1** (2001), 287–313.

[13] A.A. Abramov, A.L. Dyshko, N.B. Konyukhova, and T.V. Levitina, Evaluation of Lamé Angular wave functions by solving of auxiliary differential equations, *Comput. Math. Math. Phys.* **29** (1989), 119–131.

[14] N. Fröman and P.O. Fröman, *JWBK-approximation*, North-Holland (1965).

[15] I.V. Komarov, L.I. Ponomarev, and S.Yu. Slavyanov, *Spheroidal and Coulomb Spheroidal Functions*, (in Russian), Nauka, Moscow , 1976.

[16] M.V. Fedorjuk, Asymptotic Analysis. Linear Ordinary Differential Equations, Springer Verlag, 1993.

[17] T.V. Levitina, The conditions of applicability of an algorithm for solving two-parameter self-adjoint boundary-value problems, *Zh. Vychisl. Mat. Mat. Fiz.* **31:5** (1991), 689–697.

[18] T.V. Levitina, A numerical solution to some three-parameter spectral problems, *Zh. Vychisl. Mat. Mat. Fiz.* **39:11** (1999), 1787–1801.

[19] R. Spigler and M. Vianello, A Survey on the Liouville–Green (WKB) approximation for linear difference equations of the second order, In: Advances in difference equations, Saber N. Elaydi, I. Györi, G. Ladas (editors), Veszprem, Hungary, August 7-11, 1995, 567–577, Taylor & Francis, 1998.

[20] P. Amodio, T. Levitina, G. Settanni, and E.B. Weinmüller, On the Calculation of the Finite Hankel Transform Eigenfunctions, *J. Appl. Math. & Computing* **43** (2013), 151–173.

[21] P. Amodio and G. Settanni, A matrix method for the solution of Sturm-Liouville problems, *JNAIAM J. Numer. Anal. Indust. Appl. Math.* **6** (2011), 1–13.

[22] P. Amodio and G. Settanni, A stepsize variation strategy for the solution of regular Sturm-Liouville problems, *Numerical Analysis and Applied Mathematics, AIP Conf. Proc.* **1389** (2011), 1335-1338.

[23] P. Amodio and G. Settanni, A finite differences MATLAB code for the numerical solution of second order singular perturbation problems, *J. Comput. Appl. Math.* **236** (2012), 3869–3879.

[24] A.A. Abramov and V.I. Ulyanova, A method for solving selfadjoint multiparameter spectral problems for weakly coupled sets of ordinary differential equations, *Z*h. Vychisl. Mat. Mat. Fiz. **37:5** (1997), 566–571.

[25] L.A. Wainstein, *Open Resonators and Open Waveguides*, Soviet Radio Press, Moscow, 1966.